PROCEEDINGS, 47th Workshop on Geothermal Reservoir Engineering
Stanford University, Stanford, California, February 7-9, 2022
SGP-TR-223

In-situ Stresses and Fractures Inferred from Image Logs at Utah FORGE

Pengju Xing[1], Andy Wray[2], Edgar Ignacio Velez Arteaga[2], Aleta Finnila[3], Joseph Moore[1], Clay Jones[1], Erik Borchardt[2], John McLennan[4]

1 Energy & Geoscience Institute, University of Utah, Salt Lake City, UT, USA

2 Schlumberger

3 Golder Associates USA, Redmond, WA, USA

4 Department of Chemical Engineering, University of Utah, Salt Lake City, UT, USA

Keywords: Image logs, FMI, UBI, in-situ stresses, Utah FORGE

ABSTRACT

Image logs including Formation Micro-Imager (FMI) and Ultrasonic Borehole Imager (UBI) were acquired during or after drilling the geothermal wells at the Utah FORGE site. The static temperature measured at the toe of the injection well, 16A(78)-32, is close to 220 ^{o}C at a true vertical depth of 8560 ft. Both fractures (induced or natural) and breakouts were identified from these image logs. By interpreting the image logs, not only orientation of "horizontal" maximum principal stress was determined, but also its magnitude is constrained. The azimuth of the "horizontal" maximum principal stress is nominally NNE-SSW and the estimated magnitude largely depends on the formation's compressive strength. Based on the breakouts analysis, both normal fault and strike-slip fault regimes are possible.

1. INTRODUCTION

One injection well and five monitoring wells have been drilled at the Utah FORGE site. One of these, well 16A(78)-32 was directionally drilled at an inclination of 65^{o} to the vertical. This highly deviated well will serve as the injection leg in a doublet interconnected by hydraulic fracturing. The well was drilled to a total depth of 10,987 ft (true vertical depth 8,560 ft) and the measured static bottomhole temperature is close to 220 ^{o}C. For the offset monitoring wells; three are moderately deep with true vertical depths between ~7500 and 9500 ft.

Borehole imaging includes optical, acoustic, and electrical imaging. The main applications of borehole imaging are fractures and breakouts identification. Fractures interpreted from electrical image logs, Formation Micro-Imager (FMI), are identified by contrasts in conductivity between the fracture and the adjacent borehole wall. By contrast, fractures in acoustic image logs, Ultrasonic Borehole Imager (UBI), are associated with changes in borehole wall surface roughness or acoustic reflectivity (Davatzes and Hickman, 2005).

FMI and UBI logs were acquired during or after drilling these wells at FORGE site under higher temperature conditions than are usually experienced in oil and gas operations. Geothermal reservoir characterizations, including natural fractures assessment and in-situ stresses inference, can be obtained from the interpreted data sets. In this study, we first summarize the azimuth of induced tensile fractures, which indicates the plane containing the maximum and intermediate principal stresses. Then, we discussed the possibility of principal stresses rotation. We also calculated magnitude of the "horizontal" maximum principal stress based on observed breakouts.

2. DESCRIPTION OF THE IMAGE LOGS AT UTAH FORGE SITE

Both FMI and UBI logs were acquired during or after drilling the wells at Utah FORGE site, as listed in Table 1. Figure 1 shows an example of FMI and UBI logs from one of the monitoring wells, 78B-32. The fractures identified in the image logs can be classified as conductive continuous (wellbore through-going) fractures, conductive non-continuous fractures, and induced tensile fractures. Continuous fractures considered to be more likely of natural origin. Non-Continuous fractures may be natural in origin, drilling induced or thermally induced. We also observed interaction of the drilling and thermally induced fracturing with the existing natural fracturing. The natural fractures orientation is summarized in Finnila et al. (2021). Prominent breakouts, indicating compressive failure of the near-wellbore region, were also observed in the UBI log.

Table 1. Image logs information of wells at Utah FORGE site

Well name	Well type	True vertical depth (ft)	Image logs
16A(78)-32	Injection well	8560	ThruBit FMI, UBI
58-32	Offset monitoring well	7536	FMI
56-32	Offset monitoring well	9145	FMI
78B-32	Offset monitoring well	9500	FMI, UBI

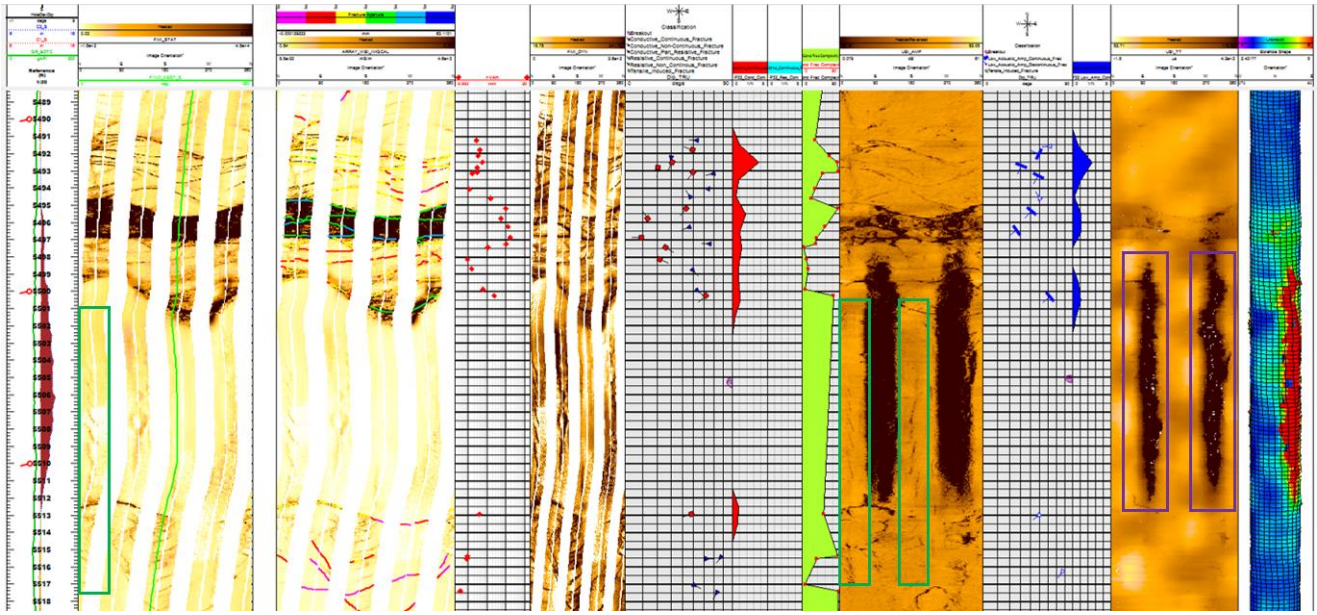

Figure 1. A composite of the FMI log and UBI log from one depth interval in well 78B-32. The red tadpoles indicate conductive continuous fractures, and the blue tadpoles indicate conductive non-continuous fractures. Green rectangle indicates induced tensile fractures while the purple rectangle shows the breakouts.

3. IN-SITU STRESSES INFERRED FROM IMAGE LOGS

3.1 Orientation of the induced tensile fractures

Induced tensile fractures from image logs suggest the plane containing the "horizontal" maximum principal stress. Figure 2 is a depth interval from the final FMI log run in well 16A(78)-32, where induced tensile fractures are identified. As summarized in Figure 3, the azimuth of induced tensile fractures is NNE-SSW.

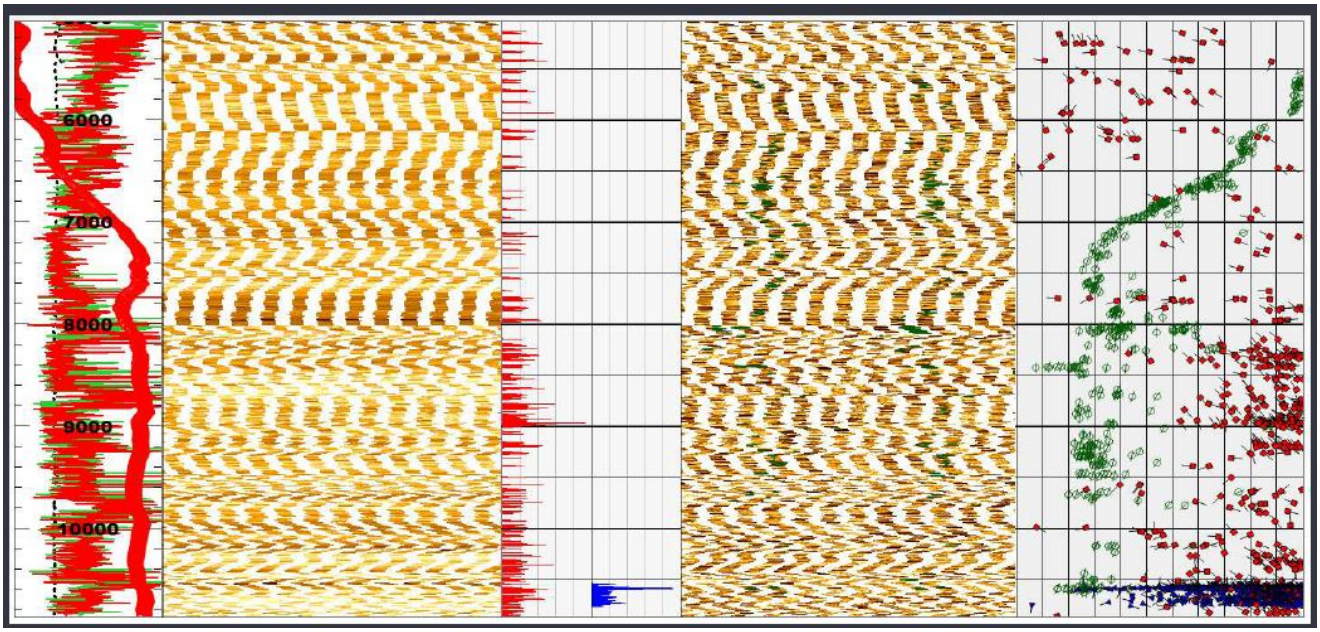

Figure 2. The overall FMI for well 16A(78)-32. Green tadpoles indicate induced tensile fractures, red tadpoles indicate conductive continuous fractures, and blue tadpoles indicate conductive non-continuous fractures (manually picked over interval 10,550-10,765ft).

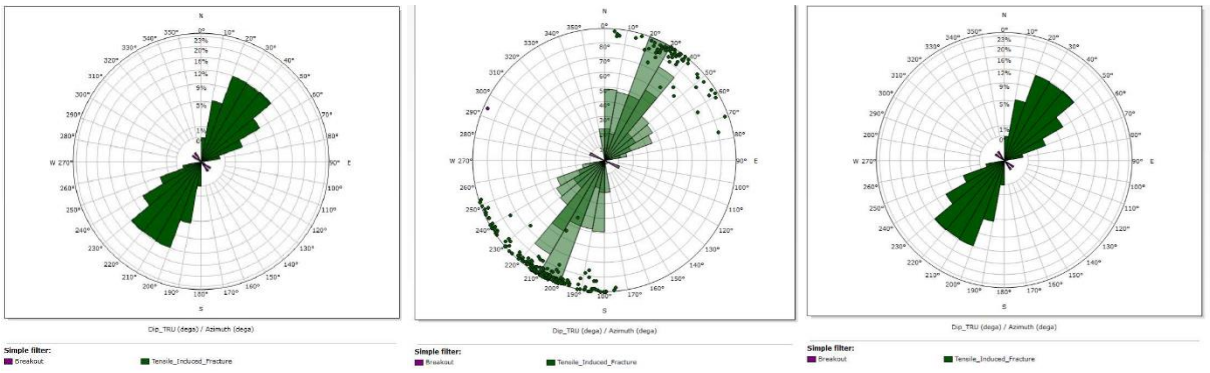

well 16A(78)-32 well 56-32 well 78B-32

Figure 3. Azimuth of induced tensile fractures from FMI logs of well 16A(78)-32, 56-32, and 78B-32.

3.2 Possible Principal Stresses Rotation

The principal stresses could be rotated and hence are not in the true vertical and horizontal directions. This should not be completely surprising based on the inferred block rotation of the Mineral Mountains, even though this is still a largely extensional basin and range setting (Bartley, 2019). Figure 4 schematically depicts the rotation of principal stress in the plane of S_v and S_{hmin}. Similarly, the stress field could also be rotated in the plane of S_v and S_{Hmax}. After rotation, the three principal stresses are not all in the vertical and horizontal directions.

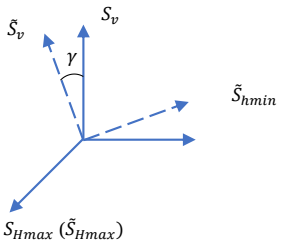

Figure 4. Rotation of the principal stresses in the plane of S_v and S_{hmin}. The dashed axes indicate the direction of principal stresses after rotation.

3.3 Maximum "horizontal" stress S_{Hmax} ($\tilde{S}_{Hmax}$) Estimation by Using Breakout Morphology

Breakouts are compressive failure on the surface of a wellbore. Breakouts are observed in the UBI logs of well 78B-32 and well 16A(78)-32. Breakout analysis is fairly well established (refer to Hickman and Zoback, 2004). First, S_{Hmax} ($\tilde{S}_{Hmax}$) is estimated through the critical orientation that breakouts can be formed, ignoring the rock strength. Then, S_{Hmax} ($\tilde{S}_{Hmax}$) is calculated based on the best estimates of the rock strength and other parameters including pore pressure and mud weight.

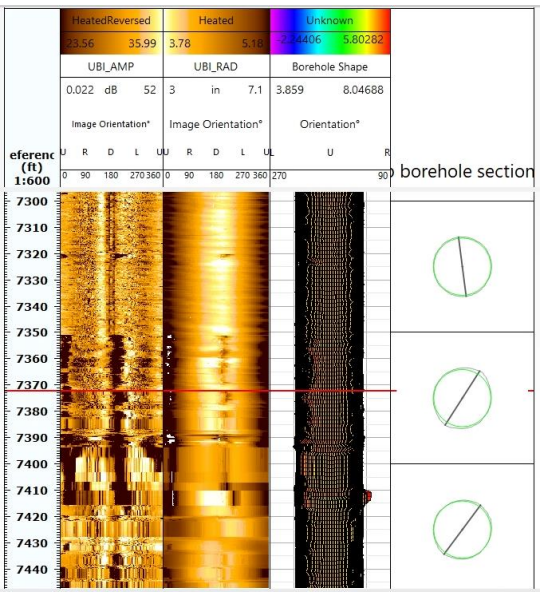

Figure 5. UBI log from one run in well 16A(78)-32. There are breakouts observed from 7350 – 7380 ft MD, which is in the inclined section of the well.

3.3.1 S_{Hmax} ($\tilde{S}_{Hmax}$) Calculated from the Critical Angle of Breakouts or Induced Tensile Fractures

Figure 5 documents the orientation of breakouts in the cross sectional view for well 16A(78)-32, which is in the inclined section. If an inclined section of a well is drilled into the plane of principle stresses, the orientation of breakouts should be from top to bottom across the wellbore section. However, the breakouts observed in the inclined section of the well 16A(78)-32 has a 30° angle with respect to the top-bottom (crown-floor) line (refer to Figure 6). This could be caused by two reasons: 1) The inclined section was actually not drilled into the principle stress plane. The well was drilled at N105°E. However, the minimum horizontal stress is anticipated to trend at N115°E. Hence, there is a 10° deviation from the inclined section of the well to S_{hmin} ($\tilde{S}_{hmin}$). 2) The principal stresses could be rotated as discussed in Section 3.2.

Breakouts are compressive failures, and hence reflect the orientation of the maximum compressive stress acting on the surface of the wellbore. Conversely induced tensile fracture will occur at the azimuthal location of the maximum tensile stress around the borehole, which is assumed to be perpendicular to the direction of related breakouts. Therefore, the critical angle of potential induced tensile fracture is 60° with σ_x (refer to Figure 6). For convenience, we calculate the critical angle of the potential induced tensile fracture, which is perpendicular to the direction of breakouts.

According to Equation 11.4 in Aadnoy and Looyeh (2010), the critical angle of an induced tensile fracture (the angle with σ_x shown in Figure 6) around borehole can be expressed as:

$$\tan 2\theta = \frac{2\tau_{xy}(\sigma_z - P_o) - 2\tau_{xz}\tau_{yz}}{(\sigma_x - \sigma_y)(\sigma - P_o) - \tau_{xz}^2 + \tau_{yz}^2} \tag{2}$$

where P_0 is the pore pressure.

As shown in Figure 7, the local stress state (x, y, z) needed in Equation (2) can be obtained through the standard transformation that is shown in Equation (3):

$$\begin{bmatrix} \sigma_x \\ \sigma_y \\ \sigma_z \\ \sigma_{xy} \\ \sigma_{xz} \\ \sigma_{yz} \end{bmatrix} = \begin{bmatrix} \cos^2\gamma\cos^2\omega & \cos^2\gamma\sin^2\omega & \sin^2\gamma \\ \sin^2\omega & \cos^2\omega & 0 \\ \sin^2\gamma\cos^2\omega & \sin^2\gamma\sin^2\omega & \cos^2\gamma \\ -\cos\gamma\cos\omega\sin\omega & \cos\gamma\cos\omega\sin\omega & 0 \\ \cos\gamma\sin\gamma\cos^2\omega & \cos\gamma\sin\gamma\sin^2\omega & -\cos\gamma\sin\gamma \\ -\sin\gamma\cos\omega\sin\omega & \sin\gamma\cos\omega\sin\omega & 0 \end{bmatrix} \begin{bmatrix} S_{Hmax} \\ S_{hmin} \\ S_V \end{bmatrix} \tag{3}$$

Note in Equation (3), if the principal stresses are rotated, the principal stresses in the right-hand side are $\tilde{S}_v$, $\tilde{S}_{Hmax}$, and $\tilde{S}_{hmin}$.

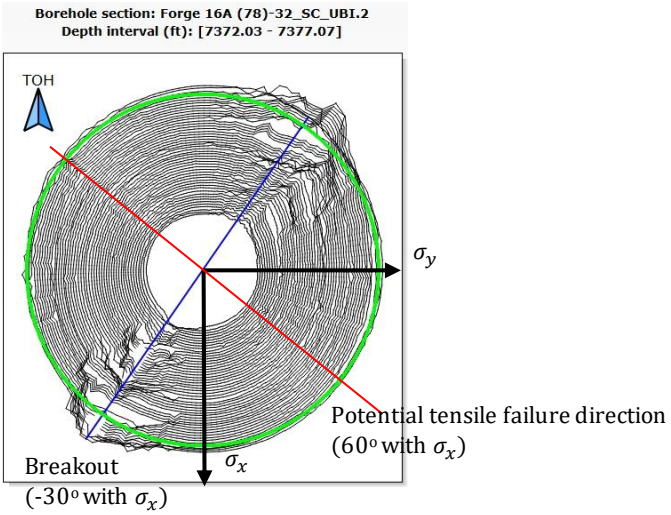

Figure 6. Cross section view of the breakouts in well 16A(78)-32 (refer to Figure 5). The angle of the breakout centerline with the top-bottom line is about 30°. The width of the breakout is 30°. The critical angle of the breakout with σ_x is -30°, and correspondingly the critical angle of the induced tensile fracture with σ_x is 60°.

Relevant parameters for calculating the critical angle are listed in Table 3. With these parameters and using Equation (2), we can obtain the relationship between the critical angle of the most tensile stress around the borehole and S_{Hmax} ($\tilde{S}_{Hmax}$), as shown in Figure 8. For the results shown in Figure 8, only the critical angle is calculated, and rock strength is ignored. Two scenarios are considered, including rotation of the principal stresses and non-rotation of the principal stresses. The breakouts shown occurred in the inclined section of well 16A(78)-32, whose angle with the vertical is 65°. In the scenario of non-rotation of principal stresses, angle γ (from S_v to wellbore axis)

should be 65°. However, in the scenario of rotation of the principal stresses, angle γ (from $\tilde{S}_v$ to wellbore axis) is 40° if the rotation angle is 25°.

For the scenario of not rotating the principal stresses ($\gamma = 65^o$), to make the critical angle of the most tensile stress to be around 60° (55° – 70°), S_{Hmax} must be in the range of 1.08 to 1.39 psi/ft. For the other scenario of rotation of principal stresses ($\gamma = 40^o$), $\tilde{S}_{Hmax}$ should be in the range of 0.84 to 1.27 psi/ft to make the critical angle of the most tensile stress to be around 60° (55° – 72°). As we can see, the required value of $\tilde{S}_{Hmax}$ is smaller for the scenario involving rotation of the principal stresses.

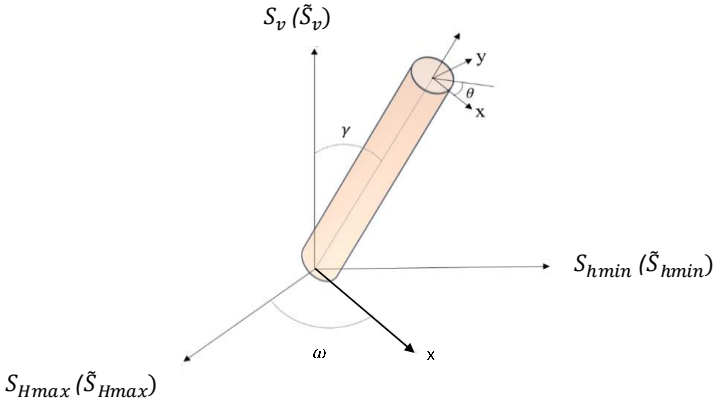

Figure 7. Stress transformation from global coordinates to the local coordinates of the wellbore.

Table 3. Parameters for the critical angle of the most tensile stress for well 16A(78)-32

Parameter	Magnitude
MD	7375 ft
TVD	7046.7 ft
Vertical Stress Gradient	1.10 – 1.16 psi/ft
Vertical stress S_v ($\tilde{S}_v$)	7751 – 8174 psi
Minimum horizontal stress gradient	0.71 – 0.79 psi/ft
Minimum horizontal stress S_{hmin} ($\tilde{S}_{hmin}$)	5503 – 5567 psi
Pore pressure gradient	0.433 psi/ft
Pore pressure P_o	3051 psi
Mud pressure gradient	9.5 ppg, 0.49 psi/ft
Mud pressure P_w	3453 psi
Angle γ (from S_v or $\tilde{S}_v$ to wellbore axis)	40° – 65° depending on the rotation of principal stresses
Angle ω (from S_{Hmax} or $\tilde{S}_{Hmax}$ to wellbore axis)*	-75°

*Note that ω is not 90° or -90° since well 16A(78)-32 was not drilled in the plane of S_v ($\tilde{S}_v$) and S_{hmin} ($\tilde{S}_{hmin}$). The well was drilled at N105°E. However, the minimum horizontal stress is anticipated to trend at N115°E. Hence, we assume that the inclined section of well 16A(78)-32 deviates 15° from S_{hmin} ($\tilde{S}_{hmin}$).

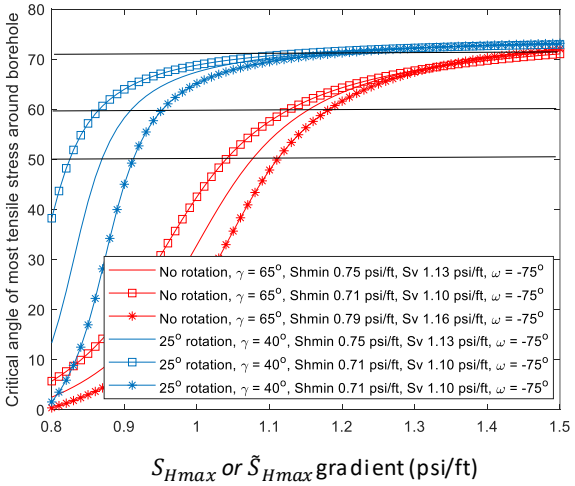

Figure 8. Relationship between the critical angle of the most tensile stress and S_{Hmax} ($\tilde{S}_{Hmax}$) gradient.

3.3.2 S_{Hmax} ($\tilde{S}_{Hmax}$) Calculated by Breakouts Considering Compressive Rock Strength

In the previous discussion, Section 3.3.1, only the critical angle to breakouts is calculated and those calculations ignored the rock's strength. Considering the unconfined compressive strength, as applicable to compressive failure via breakouts, S^*_{Hmax} can be calculated as (Equation 7.7 from Zoback, 2010): out of plane shear is not considered in this equation.

$$S^*_{Hmax} = \frac{\left(C_0 + \alpha P_o + P_w + \sigma^{\Delta T}\right) - S^*_{hmin}(1 + 2\cos 2\theta_b)}{1 - 2\cos 2\theta_b} \quad (4)$$

where:

S^*_{Hmax} ..... Maximum principal stress in the cross-section plane of wellbore
S^*_{hmax} ..... Minimum principal stress in the cross-section plane of wellbore
C_o ..... Borehole wall strength (BWS)
θ_b ..... Angle measured between S^*_{Hmax} and the edge of breakout
P_o ..... Pore pressure
α ..... Biot's coefficient
ΔP ..... Fluid pressure difference between the borehole fluid pressure and the pore pressure

Also, $2\theta_b = \pi - w_{bo}$, w_{bo} is the breakout width. Note that S^*_{Hmax} and S^*_{hmax} are in the cross-sectional plane of the wellbore. For an inclined well, S^*_{Hmax} and S^*_{hmax} are different from S_{Hmax} and S_{hmin}, and can be obtained by stress transformation described in Equation (3). $\sigma^{\Delta T}$ is the thermally induced stress, which is positive in Equation (4) when cooling. Hence, a cooling effect can result in predicting a larger S^*_{Hmax} if breakouts exist.

Parameters used in breakout calculation using Equation (4) are listed in Table 4. Here we consider the combination of parameters that gives the minimum magnitude of S_{Hmax} ($\tilde{S}_{Hmax}$). From Figure 6, we can see that the width of the breakout is about 30°. However, in this calculation a 0° breakout width is artificially used to get the lower bound of S_{Hmax} ($\tilde{S}_{Hmax}$). Similarly, the contribution of thermal cooling stress $\sigma^{\Delta T}$ is not considered either. Substituting the parameters in Table 4, Equation (4) can be reduced to:

$$S^*_{Hmax} = \frac{(C_0 + \alpha P_o + P_w) + S^*_{hmin}}{3} \quad (5)$$

Equivalent to Equation (5), breakouts can happen when the effective maximum compressive stress around the borehole σ'_{bmax} is greater than the compressive strength.

$$\sigma'_{bmax} = 3S^*_{Hmax} - S^*_{hmin} - P_w - \alpha P_o > C_0 \quad (6)$$

We rewrite equation (6) in terms of total stress:

$$\sigma_{bmax} = 3S^*_{Hmax} - S^*_{hmin} - P_w > C_0 + \alpha P_o \quad (7)$$

After stress transformation, the relationship between the maximum compressive stress around the borehole σ_{bmax} and the maximum horizontal stress gradient S_{Hmax} ($\tilde{S}_{Hmax}$) is shown in Figure 9. In this plot C_o is assumed same as unconfined compressive stress, 13200 psi measured from the core. For the case where breakouts occur, the S_{Hmax} ($\tilde{S}_{Hmax}$) gradient must be greater than 1.16 psi/ft if rotation has occurred, and greater than 1.22 psi/ft for the no rotation case. However, Tao and Ghassemi (2010) argued that C_o should be no more than 5000 psi. If C_o is low, then breakouts can occur as long as S_{Hmax} ($\tilde{S}_{Hmax}$) is greater than 0.80 psi/ft. We need to keep in mind that this is a lower bound for S_{Hmax} ($\tilde{S}_{Hmax}$) because we assumed the breakout width is zero and ignored the thermal cooling stress.

Table 4. Parameters used in breakouts calculation for well 16A(78)-32

Parameters	Magnitude
Breakout width w_{bo}	0 degrees
θ_b	90 degrees
MD	7375 ft
TVD	7046.7 ft
Pore pressure gradient	0.433 psi/ft
Pore pressure P_o	3051 psi
Mud pressure gradient	9.5 ppg, 0.49 psi/ft
Mud pressure P_w	3453 psi
$\Delta P = P_w - P_o$	402 psi
$\sigma^{\Delta T}$	Unknown but taken as zero
Borehole wall strength	13,200 psi
Biot's coefficient	0.6

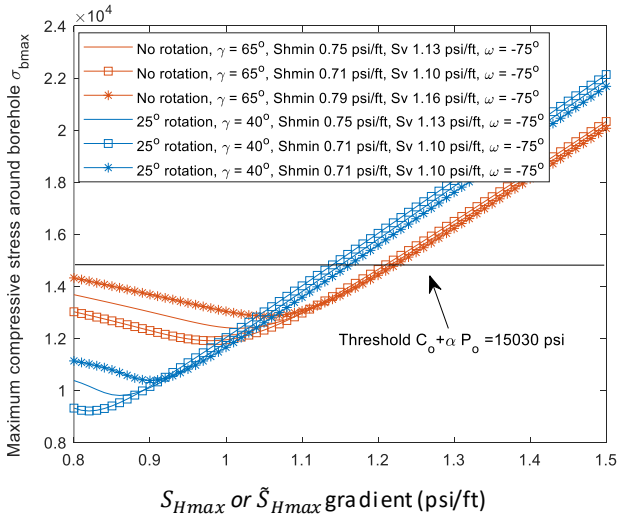

Figure 9. Relationship between the maximum compressive stress around the borehole σ_{bmax} and the maximum horizontal stress gradient S_{Hmax} ($\tilde{S}_{Hmax}$). For breakouts to occur, the S_{Hmax} ($\tilde{S}_{Hmax}$) gradient must be greater than 1.16 psi/ft for the rotation case, and greater than 1.22 psi/ft for the no rotation case. Here C_o is taken as 13200 psi.

3.3.3 Summary of S_{Hmax} ($\tilde{S}_{Hmax}$) Estimation from Breakouts

The results of S_{Hmax} ($\tilde{S}_{Hmax}$) inferred from breakouts in well 16A(78)-32 are summarized in Table 5. There are four scenarios depending on the rotation of principal stresses and rock compressive strength. In the calculations, the minimum horizontal principal stress S_{hmin} ($\tilde{S}_{hmin}$) is 0.71 – 0.79 psi/ft. S_{hmin} ($\tilde{S}_{hmin}$) is inferred from injection tests conducted in well 58-32 (Xing et al, 2020) and well 16A(78)-32 (Xing et al., 2021). The vertical principal stress S_v ($\tilde{S}_v$) is 1.10 – 1.16 psi/ft, which is calculated from the rock density. In Scenarios 1 and 3 it assumed that rock strength associated with breakouts is very low. In Scenarios 2 and 4, it assumed that C_o is equal to unconfined compressive strength (UCS). In the depths where the principal stresses appear to be rotated, Scenario 3 and 4 are considered to be the most plausible cases.

The breakouts observed from UBI logs of well 16A(78)-32 and 78B-32 are not continuous and only in several discrete sections. This could be caused by formation rock strength heterogeneity or in-situ stress heterogeneity. As shown in Table 5, breakouts tend to occur when S_{Hmax} is larger or rock strength is weaker.

The estimated S_{Hmax} ($\tilde{S}_{Hmax}$) can exceed S_v, which indicates the possibility of strike slip regime. Utah FORGE site is located in Basin and Range, which is extension and normal faulting regime. However, Strike-Slip faulting is seen in Sevier Valley region (Arabasz and Julander, 1986) and Escalante Valley (Whidden and Pankow, 2012), which are close to Utah FORGE site.

Table 5. S_{Hmax} estimated from the breakouts of well 16A(78)-32.

Scenario	Rotation of principal stresses	Rock strength C_o	Estimated S_{Hmax} ($\tilde{S}_{Hmax}$) gradient
Scenario 1	No rotation	Very weak	1.08 – 1.39 psi/ft
Scenario 2	No rotation	13200 psi	1.22 – 1.39 psi/ft
Scenario 3	25° rotation	Very weak	0.84 – 1.27 psi/ft
Scenario 4	25° rotation	13200 psi	1.16 – 1.27 psi/ft

Note: rotation could be in the plane of S_v and S_{Hmax}, or in the plane of S_v and S_{hmin}.

4. CONCLUSIONS

Fractures and breakouts are identified from the image logs acquired during or after drilling the wells at Utah FORGE site. Induced tensile fractures from the image logs suggest/confirm that the azimuth of the "horizontal" maximum principal stress is NNE-SSW. These image logs were further analyzed to constrain the magnitude of maximum "horizontal" principal stress. The discontinuous breakouts observed in the wells indicate formation heterogeneity or in-situ stresses heterogeneity at Utah FORGE site. The inference/estimation of the maximum "horizontal" principal stress largely depends on the formation's compressive strength. If unconfined compressive strength 13200 psi is used to as rock strength for breakouts calculation, S_{Hmax} ($\tilde{S}_{Hmax}$) is 1.16 – 1.39 psi. If we assume the rock is very weak, S_{Hmax} ($\tilde{S}_{Hmax}$) is 0.84 – 1.39 psi. The inferred maximum "horizontal" principal stress is smaller in the case of principal stress rotation than the case of non-rotation. The inferred S_{Hmax} shows that both normal fault and strike-slip fault regime are possible for Utah FORGE site.

ACKNOWLEDGEMENTS

Funding for this work was provided by the U.S. DOE under grant DE-EE0007080 "Enhanced Geothermal System Concept Testing and Development at the Milford City, Utah FORGE Site." We thank the many stakeholders who are supporting this project, including Smithfield, Utah School and Institutional Trust Lands Administration, and Beaver County, as well as the Utah Governor's Office of Energy Development. The authors would like to thank Stephen Hickman, Thomas Doe, and Kris Pankow for their comments.

REFERENCES

Aadnøy, B.S., 1990. In-situ stress directions from borehole fracture traces. Journal of Petroleum Science and Engineering, 4(2), pp.143-153.

Aadnøy, B. and Looyeh, R., 2010. Petroleum Rock Mechanics: Drilling Operations and Well Design. Gulf Professional Publishing.

Arabasz, W.J. and Julander, D.R., 1986. Geometry of seismically active faults and crustal deformation within the Basin and Range-Colorado Plateau transition in Utah.

Bartley JM. Joint patterns in the Mineral Mountains intrusive complex and their roles in subsequent deformation and magmatism. Geothermal Characteristics of the Roosevelt Hot Springs System and Adjacent FORGE EGS Site; Allis, R., Moore, JN, Eds. 2019:13.

Davatzes, N.C. and Hickman, S., 2005, January. Comparison of acoustic and electrical image logs from the Coso geothermal field, CA. In Proceedings, Thirtieth Workshop on Geothermal Reservoir Engineering, Stanford University (pp. 1-11).

Finnila, A., Doe, T., Podgorney, R., Damjanac, B., and Xing, P., 2021. Revisions to the Discrete Fracture Network Model at Utah FORGE Site. Geothermal Rising Conference, San Diego, California, USA, October 3-6.

Hickman, S., and Zoback, M.D. 2004. Stress orientations and magnitudes in the SAFOD Pilot Hole, Geophys. Res. Lett., 31, L15S12, doi:10.1029/2004GL020043.

Tao, Q. and Ghassemi, A., 2010. Poro-thermoelastic borehole stress analysis for determination of the in situ stress and rock strength. Geothermics, 39(3), pp.250-259.

Whidden, K.M. and Pankow, K.L., 2012. A catalog of regional moment tensors in Utah from 1998 to 2011. Seismological Research Letters, 83(5), pp.775-783.

Xing, P., McLennan, J. and Moore, J., 2020. In-Situ Stress Measurements at the Utah Frontier Observatory for Research in Geothermal Energy (FORGE) Site. Energies, 13(21), p.5842.

Xing, P., Winkler, D., Swearingen, L., Moore, J., and McLennan, J., 2021. In-Situ Stresses and Permeability Measurements from Testings in Injection Well 16A(78)-32 at Utah FORGE Site. Geothermal Rising Conference, San Diego, California, USA, October 3-6.

Zoback, M.D., 2010. Reservoir Geomechanics. Cambridge University Press.